PERGAMON

Engineering Fracture Mechanics 70 (2003) 995–1013

Engineering Fracture Mechanics

www.elsevier.com/locate/engfracmech

Size effects on flexural response of reinforced concrete elements with a nonlinear matrix

Alberto Carpinteri *, Giuseppe Ferro, Giulio Ventura

Politecnico di Torino, Department of Structural Engineering and Geotechnics, Corso Duca degli Abruzzi 24, 10129 Torino, Italy

Abstract

A dimensionless formulation of the bridged and of the cohesive crack model for reproducing the constitutive flexural response of a reinforced concrete element with a nonlinear matrix is proposed. The nonlinearity of the matrix is modelled by considering a distribution of closing forces onto the crack faces which increases the fracture toughness of the cross-section with a shielding action. The peculiarity of the models consists in the imposition of both the equilibrium and the compatibility conditions to the cracked element. The constitutive flexural response depends on three dimensionless parameters: $\widetilde{w}_c$, which controls the extension of the process zone, $N_P^{(1)}$ and $N_P^{(2)}$, related to the reinforcement phases. Eventually, some experimental and numerical examples are presented and discussed in order to validate the consistence of the proposed approach.

Keywords: High-performance concrete; Fracture mechanics; Size effects; Cohesive crack model; Bridged crack model

1. Introduction

In the last few years, growing attention for cementitious–matrix composite materials has been evidenced, in relation to the use of high-strength concretes. An important incentive to using fibers is to cut production costs by reducing, where possible, the cross-section of the element or eliminating some forms of conventional reinforcement. Recent research results have confirmed the possibility of replacing stirrups with fibers in high-strength concrete beams. On the other hand, what discourages the use of fibers in concrete is a lack of guidelines for design of structural elements made of fibrous concrete. In order to obtain a desired structural effect, an optimal combination of fibers, bars and concrete must be chosen. Moreover, the high strength of concrete and the high percentage of primary reinforcement normally adopted in the element make the experimental tests impossible at full scale with the standard jacks available in the laboratory. For that, the tests are normally realized on specimens reduced in size. This aspect appears strategical, strong size-scale effects being present. How to approach this problem is one of the main goal of the present paper. The proposed theoretical model determines the problem unknowns by considering a cracked cross-section

* Corresponding author. Tel.: +39-11-5644850/4828; fax: +39-11-5644899.
E-mail address: carpinteri@polito.it (A. Carpinteri).

0013-7944/03/$ - see front matter © 2002 Elsevier Science Ltd. All rights reserved.
PII: S0013-7944(02)00162-5

in bending and by using the local compliance and the stress-intensity factor concepts for a reinforced composite material with a nonlinear matrix. It represents an extension [8,14] of the model proposed by Carpinteri [7] and by Bosco and Carpinteri [3,9] for a discontinuous fiber distribution and by Carpinteri and Massabó [11] for a continuous one. The longitudinal reinforcements are simulated by the actions of m concentrated forces directly applied onto the crack faces. The nonlinearities of the matrix are modelled by the action of a continuous closing traction distribution onto the crack zone whose opening displacements result less than the critical value, w_c.

From dimensional analysis, the structural response, expressed by the functional relationship of moment vs. local rotation comes out to depend on three dimensionless parameters. The first parameter, $\widetilde{w}_c$, is the product of the dimensionless Young's modulus by the normalized critical crack opening displacement. The other two parameters, $N_P^{(1)}$ and $N_P^{(2)}$, called *brittleness numbers*, are related to the geometry and to the mechanical characteristics of reinforcements and matrix. The structural response depends, once all the mechanical parameters and geometrical ratios have been set, on the structural element dimension. Theoretical results confirm a transition from ductile to brittle collapse by varying the brittleness numbers N_P. It is to be observed that the dependence of the brittleness numbers on the structural dimension is represented by a power law with an exponent equal to 0.5, which is the typical exponent of the LEFM stress singularity.

2. Theoretical models

The theoretical model explains and reproduces the constitutive flexural response of a fiber-reinforced concrete element with longitudinal steel bars. Two different options for the model can be used, the *bridging* and the *cohesive*. The scheme of a cracked element is shown in Fig. 1, where h and b are the height and the thickness of the cross-section. The normalized crack depth $\xi = a/h$ and the normalized coordinate $\zeta = x/h$ are defined, x being the coordinate related to the bottom of the cross-section. In the bridging option, the distribution of the discrete actions P_i and of the continuous closing tractions $\sigma(w)$, directly applied onto the crack faces, represent the physical bridging mechanisms respectively of the longitudinal bars (primary reinforcement) and of the fibers (secondary reinforcement), acting at two different scales. Let c_i be the coordinate of the ith reinforcement from the bottom of the beam, and $\zeta_i = c_i/h$ its normalized value. Function $\sigma(w)$ is a constitutive law and defines the relation between the bridging traction, representative of the action exerted by the fibers onto the crack, and $w(x)$, the crack opening displacement at the generic coordinate x. Different laws have been considered and implemented in the numerical code, Fig. 3 [1,13,15,17]. The bridging forces of the secondary reinforcement act on the portion of the crack where the opening displacement is less than its critical value w_c. When $w > w_c$ the closing tractions vanish, Fig. 2. In the cohesive option, on the other hand, the brittle matrix and the fibers are represented as a single-phase material with homogenized properties. In this case, the closing tractions $\sigma(w)$ describe the combined restraining action of matrix and fibers on the crack opening and are given by the cohesive law of the composite material.

The assumed rigid-plastic bridging relation for the crack opening displacement w_i at the level of the ith reinforcement is suitable to describe the yielding mechanism of the reinforcement as well as the bar-matrix relative slippage (Fig. 3a). The maximum bridging traction is defined for the primary reinforcements by the ultimate force $P_{P_i} = A_i\sigma_y$ and for the fibers by the ultimate stress $\sigma_0 = \gamma\sigma_u$, A_i being the single reinforcement cross-section area, γ the fiber volume ratio, σ_y or σ_u the minimum between the reinforcement yield strength and the sliding limit for the two reinforcement phases. The stress-intensity factors, K_{IM} due to the bending moment M_F, $K_{I\sigma}$ due to the fibers and K_{Ij} due to the ith-longitudinal reinforcement, can be expressed in accordance with the two-dimensional single-edge notched-strip solution

$$K_{IM} = \frac{M}{bh^{1.5}} Y_M(\xi), \tag{1}$$

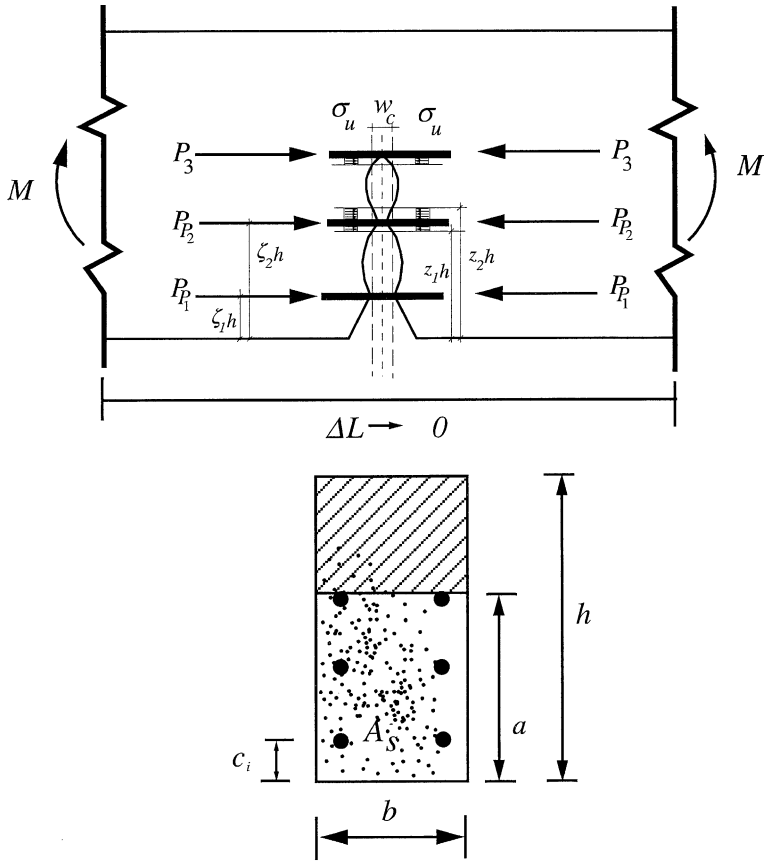

Fig. 1. Scheme of a cracked reinforced concrete element containing fibers.

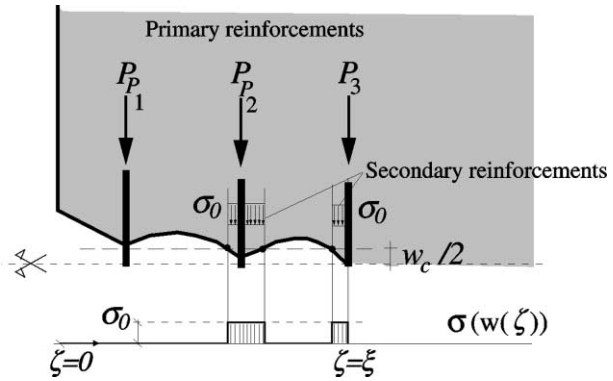

Fig. 2. Bridging actions of primary and secondary reinforcements onto the crack face.

where $Y_M(\xi)$ is a function of the relative crack depth ξ [20,22]. The factor $K_{I\sigma}$ is obtained by integrating, along the bridged crack zone, the product of the stress-intensity factor due to two opposite opening forces $P_j = 1$, applied at the generic coordinate ζ_j, times the bridging actions $\sigma(w)$

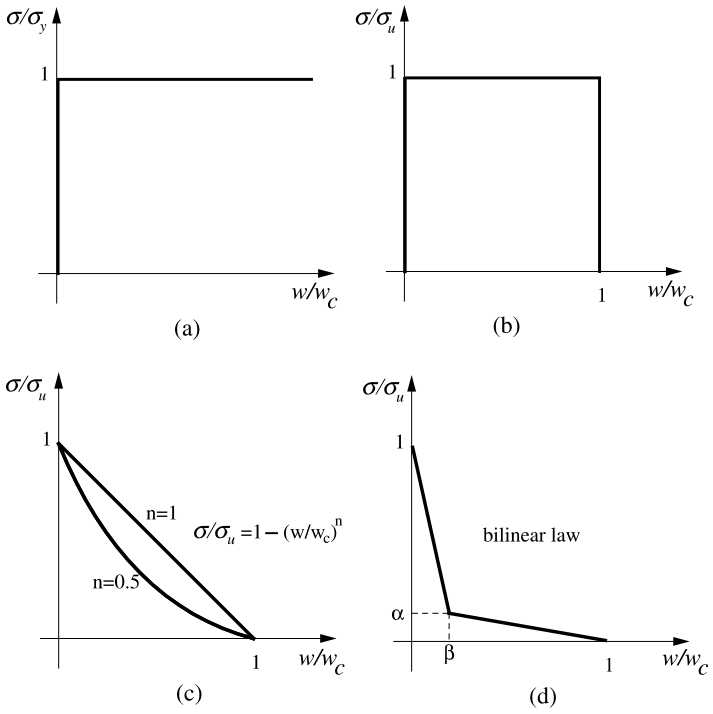

Fig. 3. (a) Rigid-perfectly plastic law for primary reinforcement; (b) perfectly plastic law with vertical drop; (c) exponential softening law; (d) bilinear softening law for secondary reinforcement.

$$K_{\mathrm{I}\sigma} = \int_0^{\xi} \frac{K_{\mathrm{I}j}}{P_j}\sigma(w(\zeta_j))bh\,\mathrm{d}\zeta_j = \frac{1}{h^{0.5}b}\int_0^{\xi}\sigma(w(\zeta_j))Y_{\mathrm{P}}(\xi,\zeta)bh\,\mathrm{d}\zeta_j, \tag{2}$$

where the integration is extended onto the whole crack, while function $\sigma(w)$ assumes nonzero values only where $w < w_{\mathrm{c}}$. For the ith longitudinal reinforcement we have

$$K_{\mathrm{I}i} = \frac{P_i}{bh^{0.5}}Y_{\mathrm{P}}(\xi,\zeta_i) \quad (i = 1,2,\ldots,m), \tag{3}$$

where $Y_{\mathrm{P}}(\xi,\zeta_i)$ is also a function of the relative crack depth ξ. The crack propagates when K_{I} is equal to the matrix toughness, K_{IC}, for the bridging option, and when K_{I} vanishes for the cohesive option

$$K_{\mathrm{I}} = K_{\mathrm{IM}} - \sum_{j=1}^{m} K_{\mathrm{I}j} - K_{\mathrm{I}\sigma} = \begin{cases} K_{\mathrm{IC}}, & \text{bridging option;} \\ 0, & \text{cohesive option.} \end{cases} \tag{4}$$

The dimensionless crack propagation moment can be obtained from Eqs. (1)–(3)

$$\frac{M_{\mathrm{F}}}{K_{\mathrm{IC}}bh^{1.5}} = \frac{1}{Y_{\mathrm{M}}(\xi)}\left\{\frac{N_{\mathrm{P}}^{(1)}}{\rho}\sum_{i=1}^{m}\rho_i\frac{P_i}{P_{P_i}}Y_{\mathrm{P}}(\xi,\zeta) + N_{\mathrm{P}}^{(2)}\int_0^{\xi}\frac{\sigma(w(\zeta))}{\sigma_0}Y_{\mathrm{P}}(\xi,\zeta)bh\,\mathrm{d}\zeta + K\right\} \tag{5}$$

with

$$N_{\mathrm{P}}^{(2)} = \frac{\gamma\sigma_{\mathrm{u}}h^{0.5}}{K_{\mathrm{IC}}} = \frac{\sigma_0 h^{0.5}}{K_{\mathrm{IC}}}, \quad \text{for } K = 1 \text{ (bridging option)}, \tag{6}$$

$$N_{\mathrm{P}}^{(2)} = \frac{1}{s} = \frac{\sigma_0 h^{0.5}}{K_{\mathrm{IC}}}, \quad \text{for } K = 0 \text{ (cohesive option)}, \tag{7}$$

where s is the brittleness number originally defined by Carpinteri [5,6], and

$$N_{\mathrm{P}}^{(1)} = \frac{\rho \sigma_{\mathrm{y}} h^{0.5}}{K_{\mathrm{IC}}}. \tag{8}$$

The parameters in the two cases assume a different physical meaning. In the bridging option, K_{IC} represents the matrix fracture toughness while in the cohesive one it represents the homogenized toughness of the composite; σ_{u} represents the ultimate strength of the secondary reinforcement in the former case while σ_0 represents the homogenized ultimate strength in the latter.

The localized rotation ϕ of the cracked cross-section can be evaluated by using Castigliano's Theorem

$$\phi = \frac{\partial U_{\mathrm{F}}}{\partial M}, \tag{9}$$

where U_{F} is the strain energy of the body due to the introduction of the crack. The relationship among U_{F}, the generalized crack propagation force, $\mathscr{G}$, the global stress-intensity factor, K_{I}, and the Young's modulus E, is

$$U_{\mathrm{F}} = \int_0^{\xi} \mathscr{G} bh \, \mathrm{d}y = \int_0^{\xi} \frac{K_{\mathrm{I}}^2}{E} bh \, \mathrm{d}y. \tag{10}$$

For a low fiber volume ratio, E can represent either the matrix or the composite material. In general, we can write

$$\phi = \frac{\partial}{\partial M} \frac{1}{E} \int_0^{\xi} \left(K_{\mathrm{IM}} - \sum_{j=1}^{m} K_{\mathrm{I}j} - K_{\mathrm{I}\sigma} \right)^2 bh \, \mathrm{d}y. \tag{11}$$

If the crack is assumed to be at the condition of incipient propagation, from Eqs. (1)–(3) and (11) we may obtain the constitutive relation between the dimensionless moment of crack propagation and the localized rotation

$$\phi = \frac{2K_{\mathrm{IC}}}{Eh^{0.5}} \left\{ \frac{M_{\mathrm{F}}}{K_{\mathrm{IC}} h^{1.5} b} \int_0^{\xi} Y_{\mathrm{M}}^2(y) \, \mathrm{d}y - \frac{N_{\mathrm{P}}^{(1)}}{\rho} \sum_{i=1}^{m} \left[\frac{P_i}{P_{P_i}} \rho_i \int_{\zeta_i}^{\xi} Y_{\mathrm{M}}(y) Y_{\mathrm{P}}(y, \zeta_i) \, \mathrm{d}y \right] \right.$$
$$\left. - N_{\mathrm{P}}^{(2)} \int_0^{\xi} \left(\int_{\zeta}^{\xi} \frac{\sigma(w(y))}{\sigma_0} Y_{\mathrm{M}}(y) Y_{\mathrm{P}}(y, \zeta) \, \mathrm{d}y \right) \mathrm{d}\zeta \right\}. \tag{12}$$

For a generic relation $\sigma(w)$, the fibers closing tractions onto the crack are indeterminate and depend on the unknown crack opening displacement function $w(x)$. The crack profile can be defined as a function of the mechanical and geometrical properties of the cross-section and of the applied loads, through Castigliano's Theorem

$$w(\zeta_k) = \lim_{F \to 0} \frac{\partial}{\partial F(\zeta_k)} \left\{ \int_0^{\xi} \frac{K_{\mathrm{I}}^2}{E} bh \, \mathrm{d}y \right\}, \tag{13}$$

where $w(\zeta_k)$ is the crack opening displacement at the generic coordinate $\zeta = \zeta_k$, F are two fictitious opening forces applied in ζ_k and K_{I} is the global stress-intensity factor

$$K_{\mathrm{I}} = K_{\mathrm{IM}} - \sum_{j=1}^{m} K_{\mathrm{I}j} - K_{\mathrm{I}\sigma} + K_{\mathrm{IF}} \tag{14}$$

in which K_{IF} is the stress-intensity factor due to the forces F. The normalized crack opening displacement assumes the following form, by substituting the specific expressions of the stress-intensity factors

$$\widetilde{w}(\zeta_k) = \frac{2K_{IC}h^{0.5}}{E}\left\{\frac{M_F}{K_{IC}h^{1.5}b}\int_{\zeta_k}^{\xi} Y_M(y)Y_P(y,\zeta_k)\,dy - \frac{N_P^{(1)}}{\rho}\sum_{i=1}^{m}\left[\frac{P_i}{P_{P_i}}\rho_i\int_{\max[\zeta_i,\zeta_k]}^{\xi} Y_P(\zeta_i,y)Y_P(y,\zeta_k)\,dy\right]\right.$$
$$\left. - N_P^{(2)}\int_{\zeta_k}^{\xi}\left(\int_0^y \frac{\sigma(w(\zeta))}{\sigma_0}Y_P(y,\zeta)\,d\zeta\right)Y_P(y,\zeta_k)\,dy\right\} \tag{15}$$

in which the last term represents the displacement at the abscissa ζ_k due to the distribution of tractions $\sigma(w)$, between 0 and ξ. Eqs. (12) and (15) set up a statically indeterminate nonlinear problem. The reactions P_i and $\sigma(w)$ are evaluated by using the numerical procedure reported in the following, which is based on the assessment of kinematic compatibility and static equilibrium equations. The complete description of the computational algorithm is reported in Section 4.

3. Dimensional analysis

The analytical formulation has been developed in a dimensionless form to define the parameters that synthetically control the behaviour of the cross-section in bending. A fundamental set of dimensionally independent variables has been chosen, i.e. K_{IC} [F][L]$^{-1.5}$ and h [L] [4]. The dimensionless groups proposed in the theoretical formulation, $K_{IC}/(\sigma_u h^{0.5})$ and $M_F/(K_{IC}h^{1.5}b)$, have been obtained by multiplying the different variables involved in the physical problem by a suitable combination of the fundamental set. The number of dimensionless parameters controlling the mechanical behaviour depends at first on the assigned bridging or cohesive relation $\sigma(w)$. If this relation is rigid-plastic, Fig. 3b, the closing tractions are uniform and constant along the fictitious crack faces during the entire loading process. In the absence of the primary reinforcement, the traction-free crack depth ξ_r is equal to the depth of the initial notch. In that case, the constitutive flexural relationship can be evaluated through the equilibrium condition alone [12]. If the geometrical ratios are kept constant, the brittleness number $N_P^{(2)} = 1/s$ proves to be the single parameter controlling the behaviour of the cross-section. When, instead, two reinforcing phases are present, and a generic bridging or cohesive law with a critical crack opening displacement w_c is considered, the problem is statically indeterminate and the compatibility must be satisfied. To define the parameters controlling the behaviour for the above assumption, in addition to relations (5) and (12), reference should be made to the propagation condition for the traction-free crack, which controls the extension of the bridging or cohesive zone. The presence of the primary reinforcement complicates the problem, as along any interval between two bars a zone with crack opening displacement greater than its critical value can be found, Fig. 2. The traction-free crack propagates when the crack opening displacement reaches the critical value w_c. From Eq. (15), we can write

$$\frac{1}{2}\widetilde{w}(\zeta_k) = \frac{M_F}{K_{IC}h^{1.5}b}\int_{\zeta_k}^{\xi} Y_M(y)Y_P(y,\zeta_k)\,dy - \frac{N_P^{(1)}}{\rho}\sum_{i=1}^{m}\left[\frac{P_i}{P_{P_i}}\rho_i\int_{\max[\zeta_i,\zeta_k]}^{\xi} Y_P(\zeta_i,y)Y_P(y,\zeta_k)\,dy\right]$$
$$- N_P^{(2)}\int_{\zeta_k}^{\xi}\left(\int_0^y \frac{\sigma(w(\zeta))}{\sigma_0}Y_P(y,\zeta)\,d\zeta\right)Y_P(y,\zeta_k)\,dy. \tag{16}$$

This condition is verified at each iteration of the procedure described in the next section. It refers the fact that, for an assigned generic bridging or cohesive law, if geometrical similarity is assumed, another dimensionless parameter, i.e.

$$\widetilde{w}_c = \frac{E w_c}{K_{IC} h^{0.5}}, \tag{17}$$

controls the composite flexural response. The functional constitutive relationship can be given the general form

$$f\left(\frac{M}{K_{IC} h^{1.5}}, \widetilde{\phi}, N_P^{(1)}, N_P^{(2)}, \widetilde{w}_c\right) = 0. \tag{18}$$

This relation has a general validity for both the model options. Nevertheless, for the cohesive option, the brittleness number $N_P^{(2)} = 1/s$ and the parameter $\widetilde{w}_c$ are not independent variables. This is due to the relationship between the homogenized fracture toughness K_{IC} of matrix and secondary phase reinforcement, and the fracture energy $\mathscr{G}_F$

$$K_{IC} = \sqrt{\mathscr{G}_F E} \quad \text{where } \mathscr{G}_F = \int_0^{w_c} \sigma(w)\,dw. \tag{19}$$

The composite fracture toughness is, in other words, linked, through Irwin's relationship, to the composite fracture energy, which is defined by the area beneath the cohesive curve $\sigma(w)$. If the cohesive power-law: $\sigma/\sigma_u = 1 - (w/w_c)^n$ is assumed (Fig. 3c), the following relationship holds:

$$\frac{K_{IC}^2}{E} = \int_0^{w_c} \sigma(w)\,dw = \frac{n}{n+1}\sigma_u w_c. \tag{20}$$

If $\widetilde{E} = (E h^{0.5})/K_{IC}$ is the dimensionless Young's modulus, the dimensionless parameter $\widetilde{w}_c$ of Eq. (17) can be expressed, by means of Eq. (20), as a function of the brittleness number s, and the relation is

$$\widetilde{w}_c = \frac{n}{n+1}\frac{s}{\widetilde{E}}. \tag{21}$$

In the case of a bilinear law (Fig. 3d), the relation between $\widetilde{w}_c$ and s is the following:

$$\widetilde{w}_c = s\frac{2}{\beta + \alpha}. \tag{22}$$

As a consequence, the dimensionless functional relationship (17) for the cohesive model becomes

$$f\left(\widetilde{M}, \widetilde{\phi}, N_P^{(1)}, N_P^{(2)}\right) = 0, \tag{23}$$

where $N_P^{(1)}$ and $N_P^{(2)}$ are the governing parameters.

In conclusion, if the theoretical problem is analyzed via the bridging option of the proposed model, and the material is modeled as multiphase, three parameters, $N_P^{(1)}$, $N_P^{(2)}$ and $\widetilde{w}_c$ control the mechanical response of the cross-section. On the other hand, if the theoretical problem is analyzed via the cohesive option, which homogenizes the composite material, two parameters $N_P^{(1)}$ and $N_P^{(2)}$ affect the kind of structural response. Physical similitude in the structural response is predicted when the dimensionless parameters are kept constant, although the single mechanical and geometrical properties vary.

4. Description of the algorithm

The computation of the bending moment M_F and of the relative rotation ϕ between the faces of the crack for a given crack depth ξ is carried out by using the following fundamental relationships:

$$\begin{aligned} &\{P\} = \{P(\{w\}, \sigma)\}, \\ &\{w\} = \{w(\{P\}, \sigma)\}, \\ &w(\zeta) = w(\zeta, \{P\}, \sigma). \end{aligned} \tag{24}$$

These equations give respectively:

- the tractions at the m primary reinforcements (bars) as functions of the corresponding openings and of the cohesive closing stresses;
- the openings at the primary reinforcements as functions of their tractions and of the cohesive closing stresses;
- the opening at a generic abscissa ζ as a function of the primary reinforcement tractions and of the cohesive closing stresses.

It is to be noted explicitly that the equations $\{P\} = \{P(\{w\}, \sigma)\}$ and $\{w\} = \{w(\{P\}, \sigma)\}$ are not one the inverse of the other even in the noncohesive case, i.e. even if $\sigma(\zeta) = 0\ \forall \zeta \in [0, \xi]$. This is a consequence of the rigid-plastic constitutive law for the primary reinforcements, stating that for the ith reinforcement it is $w(\zeta_i) = 0$ if $P_i < P_{P_i}$, and $w(\zeta_i) = w(\zeta_i, \{P\}, \sigma)$ if $P_i = P_{P_i}$.

The iterative algorithm for implementing the proposed model is structured on a two-level computation:

- an external iteration computing the tractions and the openings at the m primary reinforcements;
- an internal iteration computing the distribution and extension of the cohesive intervals.

4.1. External iteration

In the external iteration the tractions/openings at the reinforcement bars are determined according to their rigid-plastic costitutive law for a given crack depth ξ and for some assumed distribution of the closing stresses along the crack faces. This distribution is updated in the internal iteration according to the costitutive law of the matrix/secondary reinforcement. The following description of the iteration algorithm is general, and applies to the three cases:

- only primary reinforcement is present ($N_{\mathrm{P}}^{(1)} \neq 0$, $N_{\mathrm{P}}^{(2)} = 0$);
- only secondary reinforcement is present ($N_{\mathrm{P}}^{(1)} = 0$, $N_{\mathrm{P}}^{(2)} \neq 0$);
- both primary and secondary reinforcement are present ($N_{\mathrm{P}}^{(1)} \neq 0$, $N_{\mathrm{P}}^{(2)} \neq 0$).

A loop is performed over the m primary reinforcements, from the farthest to the closest to the crack tip. If the stress level at a certain reinforcement exceeds the maximum, then at this reinforcement the maximum stress is assigned and the relevant opening is computed. These assigned and computed data are used to recompute the stresses in the bars closest to the tip. The detailed flow follows:

(1) initialization;
(2) if $N_{\mathrm{P}}^{(2)} \neq 0$ the extension of the cohesive intervals is set to all;
(3) if $N_{\mathrm{P}}^{(1)} \neq 0$ the openings at the m primary reinforcements are set equal to zero, $\{w\} = \{0\}$, and a convergence tolerance $\mathrm{tol_e}$ is fixed;
(4) loop (the apex (k) indicates the kth iteration)
   (a) the stresses at the primary reinforcements are computed, $\{P\}^{(k)} = \{P(\{w\}, \sigma)\}$;
   (b) the stresses exceeding or nearby the maximum are set equal to it $P_i = \min(P_i + \mathrm{tol_e}, P_{P_i})\ i = 1, \ldots, m$. Here the role of the tolerance $\mathrm{tol_e}$ is the one of eliminating observed oscillations in the convergence process;

(c) the current value of the tractions $\{P\}^{(k)}$ is used to compute the norm of the variation of the primary reinforcements stresses $\mathscr{N}_e = \|\{P\}^{(k)} - \{P\}^{(k-1)}\|_{+\infty}$. The (plus infinity) norm $\|\dots\|_{+\infty}$ is defined as the maximum absolute value in the components of the argument vector;
(d) if $N_P^{(2)} \neq 0$ then go to the internal iteration for the computation and updating of the distributed closing stresses (secondary reinforcement);
(e) loop exiting condition in the case $N_P^{(2)} \neq 0$, $N_P^{(1)} = 0$. In this case, as no interaction is present with the primary reinforcement (being it absent) and all the computations are carried out in the internal iteration, the loop is exited immediately;
(f) loop convergence check in the case $N_P^{(2)} \neq 0$, $N_P^{(1)} \neq 0$. If $\mathscr{N}_e < \mathrm{tol}_e\|\{P_P\}\|_{+\infty}$, the algorithm has converged and the loop is exited;
(g) loop for $i = 1 \dots m$ (openings and primary reinforcement tractions update)
  (i) if $P_i^{(k)} = P_{P_i}$ then compute the opening $w(\zeta_i) = w(\zeta_i, \{P\}^{(k)}, \sigma)$ and recompute the stresses at the primary reinforcements, $\{P\}^{(k)} = \{P(\{w\}, \sigma)\}$, else $w(\zeta_i) = 0$ and $P_i^{(k)} = \max(0, P_i^{(k)})$;
  (ii) set $P_i^{(k)} = \min(P_i^{(k)}, P_{P_i})$;
(h) end loop i;
(i) $\mathscr{N}_e = \|\{P\}^{(k)} - \{P\}^{(k-1)}\|_{+\infty}$;
(j) loop convergence check in the case $N_P^{(2)} = 0$, $N_P^{(1)} \neq 0$. If $\mathscr{N}_e < \mathrm{tol}_e\|\{P_P\}\|_{+\infty}$, the algorithm has converged and the loop is exited;

(5) return to step 4.

4.2. Internal iteration

For a fixed value of the tractions at the primary reinforcements and of the corresponding openings $\{w\}$, the internal iteration computes the extension of the cohesive intervals and applies the secondary reinforcement (or matrix) constitutive law. The extension of the cohesive intervals is determined by a couple of abscissas for each primary reinforcement, setting the related lower and upper limit of the cohesive interval. The crack tip is treated algorithmically in the same way, in the sense that it has associated a couple of cohesive abscissas, the lower representing the extension of the cohesive interval below the crack tip, and the second being always coincident with the crack tip itself, Fig. 1. Consequently, if m is the number of primary reinforcements, the number of interval extrema is globally $2m + 2$ and the $m + 1$ cohesive intervals are determined by $[\{z_c\}_{i-1}, \{z_c\}_i]$, $i = 2, 4, \dots, 2m + 2$. Here $\{z_c\}$ is the vector storing the abscissas, and it is always sorted in ascending order: $\{z_c\}_i \leqslant \{z_c\}_{i+1}$, $i = 1, 3, \dots, 2m + 1$.

In the general case, $\{w\} = \{w(\{P\}, \sigma)\}$ is an integral equation, σ being a function of the opening by the constitutive law, $\sigma = \sigma(w)$. For this reason the stresses are computed considering the displacements at the previous iteration. When convergence is reached, the difference between the two is, of course, negligible. To save the displacements at the previous iteration, the crack is subdivided into $m + 1$ zones where the displacement is a continuous and differentiable function. In the case of a single primary reinforcement ($m = 1$) the first zone extends from the abscissa zero to the one of the first primary reinforcement z_1, and the second zone extends from z_1 to the crack tip ξ. Into each zone the displacements are stored in the form of a concavity preserving spline interpolation with variable number of breakpoints. The spline interpolation w_s computed at an iteration is used in the subsequent iteration to approximate the closing stresses through the constitutive relation $\sigma = \sigma(w) \cong \sigma(w_s)$. This approach is an evolution of the one proposed by Carpinteri and Massabó [12], where a simple spline was used to interpolate the closing stresses σ. In that case difficulties arose because the concavity of the interpolation could contradict the one of the data, especially when nondifferentiable constitutive laws are used.

The internal iteration algorithm described in the following is a form of the binary search (bisection) algorithm on the abscissas of the cohesive intervals $\{z_c\}$ applied to each of the $m + 1$ zones in which the

crack is subdivided. The ith zone contains the superior extremum z^{s} of the $(i-1)$th interval and the inferior extremum z^{i} of the ith interval. Two convergence measures are evaluated: $\mathscr{N}_z = \|\{z_c\}^{(k-1)} - \{z_c\}^{(k)}\|_{+\infty}$, accounting for the variation of the cohesive intervals between two subsequent iterations, and $\mathscr{N}_s = \|\{w_s(\{z_c\})\}^{(k)} - \{w(\{z_c\})\}\|_{+\infty}$, accounting for the precision of the spline interpolation vs. the exact displacement measured at the extrema of the cohesive intervals.

The internal iteration loop structure is the following:

(1) compute the spline concavity preserving interpolation on the $m+1$ zones (nine sampling points/zone are used);
(2) loop over the $m+1$ zones, from the closest to the crack tip to the farthest;
   (a) if $w(z^{s}) < w_c$ then the cohesive interval is enlarged by bisection on the right, else the cohesive interval is reduced by bisection on the left;
   (b) if $w(z^{i}) < w_c$ then the cohesive interval is enlarged by bisection on the left, else the cohesive interval is reduced by bisection on the right;
(3) end loop on the zones;
(4) the vector $\{z_c\}$ is sorted in ascending order. This is necessary because the abscissas updating by bisection can produce overlapping cohesive intervals, which are eliminated in this step;
(5) compute the norms $\mathscr{N}_z$ and $\mathscr{N}_s$ and check for the convergence condition;
(6) if not converged go to step 1.

5. Simulations and size-effects

In the flexural behaviour of a reinforced composite material with a nonlinear matrix, a size-scale effect can be evidenced. This effect consists of variations in the shape of the constitutive flexural relationship when the beam depth varies. This aspect, as previously mentioned, is very important when experimental results obtained on small specimens have to be extrapolated to full scale structures. In fact, for high-strength concrete with fibers and an high primary reinforcement percentage, it results very hard to perform experimental tests on full size elements.

To analyze this phenomenon, the bridging option of the proposed theoretical model has been applied assuming for the secondary reinforcement the bridging relation, $\sigma(w) = \gamma\sigma_u$ if $w = w_c$ and $\sigma(w) = 0$ if $w > w_c$. The flexural behaviour of the cross-section is controlled by the three parameters $N_P^{(1)}$, $N_P^{(2)}$ and $\widetilde{w}_c$. If only the size-scale effect is of interest, the mechanical properties can be assumed constant (K_{IC}, E, $\rho\sigma_y$, $\gamma\sigma_u$, w_c). Therefore, the products of each of the two brittleness numbers $N_P^{(1)}$, $N_P^{(2)}$, times $\widetilde{w}_c$

$$N_P^{(1)}\widetilde{w}_c = \frac{\rho\sigma_y h^{0.5}}{K_{IC}}\frac{Ew_c}{K_{IC}h^{0.5}} = \frac{\rho\sigma_y E w_c}{K_{IC}^2} = \frac{\rho\sigma_y w_c}{\mathscr{G}_F}, \tag{25}$$

$$N_P^{(2)}\widetilde{w}_c = \frac{\gamma\sigma_u h^{0.5}}{K_{IC}}\frac{Ew_c}{K_{IC}h^{0.5}} = \frac{\gamma\sigma_u E w_c}{K_{IC}^2} = \frac{\gamma\sigma_u w_c}{\mathscr{G}_F}, \tag{26}$$

which do not depend on the depth of the cross-section, result to be constant.

In order to show the effect of the element size on the flexural response, the following example has been analyzed. Let consider six geometrically similar elements, with h between 10 and 1000 mm. The beams are characterized by a single reinforcement bar located at $0.1h$ from the bottom of the beam, with reinforcement ratio equal to 1% and yield stress $\sigma_y = 240\ \mathrm{N\,mm^{-2}}$, elastic modulus $E = 30\,000\ \mathrm{N\,mm^{-2}}$, cementitious matrix toughness $K_{IC} = 64\ \mathrm{N\,mm^{-3/2}}$, and volume ratio of fibers embedded in the matrix equal to 1%

Table 1
Dimensionless parameters by varying the beam depth h

h (mm)	$N_P^{(1)}$	$N_P^{(2)}$	$\widetilde{w}_c$
10	0.119	0.054	1482
20	0.168	0.077	1048
50	0.265	0.121	663
100	0.375	0.172	469
500	0.839	0.384	210
1000	1.186	0.544	148

($\sigma_u = 110$ N mm^{-2}). With these mechanical parameters the two ratios in Eqs. (25) and (26) assume respectively the values 187 and 86. By varying h, the three dimensionless parameters assume the values reported in Table 1. The evolutive process of crack propagation expressed in terms of the dimensionless crack propagation moment, $M_F/(K_{IC}h^{1.5}b)$, vs. the normalized crack depth, $\xi = a/h$, is reported in Fig. 4a for the six cases. For $0 < \xi < \zeta_1$, the crack crosses only the matrix. The strain-softening response is controlled by the matrix toughness and by the secondary reinforcements. For crack depths tending to zero, an infinite resistance is provided, as expected from LEFM. In correspondence of $\xi = \zeta_1 = 0.1$, when the crack reaches the primary reinforcement, a loading drop is evidenced [2]. For the smallest sizes, the response is unstable and an uncontrollable crack propagation can be avoided only by decreasing the applied load. On the other hand, for the largest sizes, the process is stable, and a slow crack growth is possible also by increasing the applied load. The crack propagation moment vs. local rotation diagram is reported in Fig. 4b. The crack propagation moment shows a vertical asymptote for $\phi \to 0$ ($\xi \to 0$). A vertical drop is achieved when the crack crosses the primary reinforcement. For $h \geqslant 100$ mm, a snap-through instability is present after the drop (dotted line), which is less and less evident for increasing size, and an evident hardening portion develops. On the other hand, for $h = 20$ and 10 mm the flexural behaviour is brittle, and a monotonically decreasing branch follows the peak moment. Therefore, to predict the structural behaviour of a beam element with beam depth $h = 500$ mm, bar reinforcement percentage equal to 1%, and fibers percentage of 1%, by an experimental test on a beam scaled 1:10 ($h = 50$ mm), the latter should have a steel percentage equal to 3.16% and a fiber reinforcement ratio of 3.16% in order to have the same flexural behaviour. In other words, the reinforcement percentage, as well as the fiber percentage, when the remaining mechanical parameters are fixed, must be scaled as $h^{-0.5}$, for the brittleness numbers remaining the same.

6. Experimental results and numerical simulations

The bridged crack model has been used to simulate some experimental results reported in [21]. Two different three point bending tests have been considered, related to beams having the same geometry and tension steel reinforcement. The two tests are denominated DR30 and DR32 in [21] and differ in the fiber volume ratio. While the beam DR30 is made by plain concrete, the beam DR32 has 1% fiber volume ratio. The beams have rectangular cross-section (130×203 mm) and a total length of 2500 mm. The distance between the supports is 2250 mm. The tension reinforcement is constituted by 2Ø12 of high-strength steel bars (yield strength = 617 N mm^{-2}). The steel percentage is $\rho = 0.99\%$ of the cross-section area, as reported by the authors, if the area is computed assuming as height the distance between the bars and the upper side of the cross-section (176 mm, see Fig. 1 in [21]). According to the model presented in this paper, the steel percentage is referred to the total cross-section area, so that the steel percentage to be considered is $\rho = 0.86\%$.

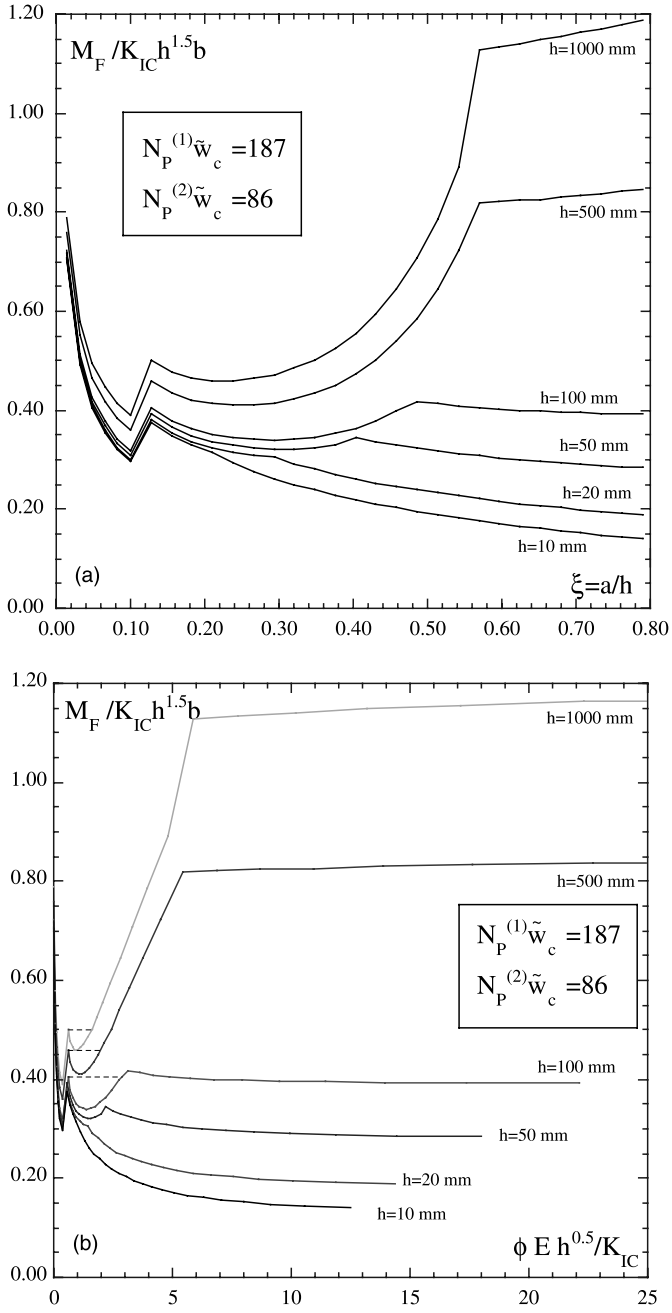

Fig. 4. (a) Dimenxsionless crack propagation moment vs. normalized crack depth for beam depths varying between 10 and 1000 mm; (b) dimensionless crack propagation moment vs. normalized local rotation.

In the definition of the displacement at the primary (tension steel) reinforcement, Eq. (16), the localized compliances

$$\lambda_{iM} = \frac{2}{hbE}\int_{\zeta_i}^{\xi} Y_{\mathrm{P}}(y,\zeta_i)\,Y_{\mathrm{M}}(\xi)\,\mathrm{d}y, \tag{27}$$

$$\lambda_{ij} = \frac{2}{bE}\int_{\max[\zeta_i,\zeta_j]}^{\xi} Y_{\mathrm{P}}(y,\zeta_i)\,Y_{\mathrm{P}}(y,\zeta_j)\,\mathrm{d}y \tag{28}$$

are introduced. The two integrals (Eqs. (27) and (28)) are improper because of the singularity of the integrand function at $\xi = \zeta_i$, Eq. (27), and at $\xi = \max[\zeta_i, \zeta_j]$, Eq. (28). While the integral (27) converges to a finite value, the integral (28) diverges. This problem has been investigated by Carpinteri and Massabó [10], who also provided a physically sound solution for this problem. Based on the observation that the reinforcement traction is not punctual but distributed over a length equal to the diameter of the bar, the compliance can be written in the form

$$\lambda_{iP_i} = \frac{2}{Eb\tilde{d}}\int_{\zeta_i}^{\xi}\int_{\zeta_i-\tilde{d}/2}^{\min[y,\zeta_i+\tilde{d}/2]} Y_{\mathrm{P}}(y,\zeta)\,\mathrm{d}\zeta\,Y_{\mathrm{P}}(y,\zeta_i)\,\mathrm{d}y, \tag{29}$$

$\tilde{d} = d/h$ being the nondimensional bar diameter. Carpinteri and Massabó [10], suggested to eliminate the singularity in Eq. (28) by translating the lower integration limit by a quantity t. In such a way, when $i = j$, it is assumed

$$\lambda_{ii} = \frac{2}{Eb}\int_{\zeta_i+t/h}^{\xi} Y_{\mathrm{P}}(y,\zeta_i)^2\,\mathrm{d}y. \tag{30}$$

The nondimensional quantity $\tilde{t} = t/h$ has been called cutoff by Carpinteri and Massabó [10], and it is determined by equating Eqs. (29) to (30)

$$\frac{2}{Eb\tilde{d}}\int_{\zeta_i}^{\xi}\int_{\zeta_i-\tilde{d}/2}^{\min[y,\zeta_i+\tilde{d}/2]} Y_{\mathrm{P}}(y,\zeta)\,\mathrm{d}\zeta\,Y_{\mathrm{P}}(y,\zeta_i)\,\mathrm{d}y = \frac{2}{Eb}\int_{\zeta_i+t/h}^{\xi} Y_{\mathrm{P}}(y,\zeta_i)^2\,\mathrm{d}y. \tag{31}$$

This equation can be solved for $\tilde{t}$. It comes out that the value of $\tilde{t}$ is not sensitive to the position of the bar and the crack depth, while is mainly influenced by the bar diameter d.

The ratio between the bar diameter and the total height of the cross-section is equal in this case to 0.059, so that the computation of the nondimensional cutoff yields 0.0026.

The model produces as a result the values of the nondimensional bending moment and rotation as functions of the crack depth. For comparison with the experimental results these values have been converted into displacement vs. load diagrams. The conversion is realized by considering the scheme of Fig. 5, where a three point bending test is depicted. The displacement at midspan of the beam is supposed as given by the elastic part plus a rigid part due to the concentrated rotation of the cracked section. From the definition of nondimensional bending moment and rotation, we can write

$$M_{\mathrm{F}} = \widetilde{M} K_{\mathrm{IC}} b h^{1.5}, \tag{32}$$

$$\phi = \frac{\tilde{\phi} K_{\mathrm{IC}}}{E h^{0.5}}. \tag{33}$$

Consequently, the vertical load and displacement at midspan are given by

$$P = \frac{4M_{\mathrm{F}}}{L}, \tag{34}$$

$$\delta = \delta_{\mathrm{el}} + \delta_{\phi} = M_{\mathrm{F}}\frac{L^2}{48E^*I} + \frac{\phi L}{4}, \tag{35}$$

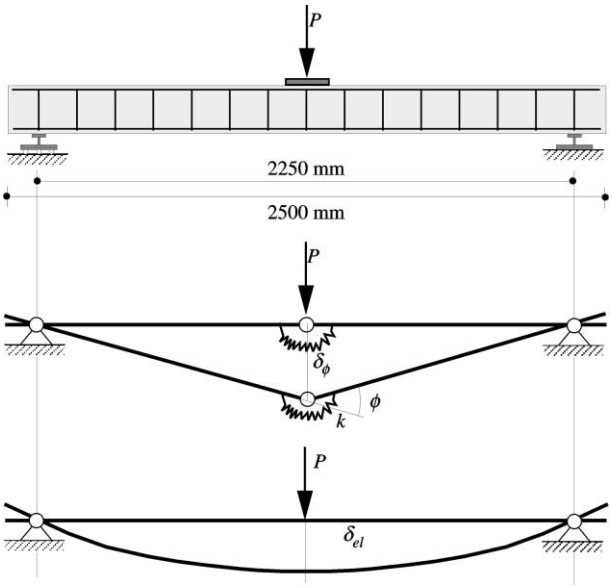

Fig. 5. Details of test beams and plastic hinge formation [21].

where the inertia is related to the total cross-section, L is the span length, and $E^* = E/2.2$, E being the conventional 28 days static modulus. This assumption is known in the literature, e.g. [5,16], and takes into account the nonlinear material behavior in the zone ahead the crack tip. For the beam DR30 the modulus E^* is then considered equal to 12.786 kN mm^{-2}.

Observing the experimental results reported in [21], it has been noticed that the load vs. displacement diagram for the beam DR30 must be referred to a tension steel with a resistance higher than the reported one (617 N mm^{-2}). In fact, the maximum load corresponds to a bending moment at midspan whose value is higher than the effective height of the cross-section times the traction at the steel reinforcement. For this reason a tension steel reinforcement strength equal to 725 N mm^{-2} has been considered in the simulations.

Therefore, for the beam DR30, assuming a matrix toughness $K_{IC} = 35.76$ N mm$^{-3/2}$, the brittleness number $N_P^{(1)}$ is given by

$$N_P^{(1)} = \frac{\rho \sigma_y \sqrt{h}}{K_{IC}} = 2.484. \tag{36}$$

The experimental and computed load vs. displacement diagrams are reported in Fig. 6. The numerical simulation has been carried out using the bridging option, as the fibers were not present in this case. The results of the model do not catch the progressive decrease of the tangent modulus due to concrete damage, although reproduce closely the qualitative behavior of the structural member as well as the limit load. The latter result is due to assumed steel strength.

The mechanical parameters adopted for the beam DR30, have been used for the simulation of the test DR32, where crimped steel fibers have been added to concrete. The steel fibers are characterized by a length equal to 50 mm, a diameter equal to 0.5 mm, a strength of 1050 N mm^{-2} and are mixed with concrete with a percentage of 1%. A first reduction factor of 1/3 is to be assumed for the fiber volume percentage, for taking into account the random spatial distribution of the fibers inside the matrix. This simple assumption is based

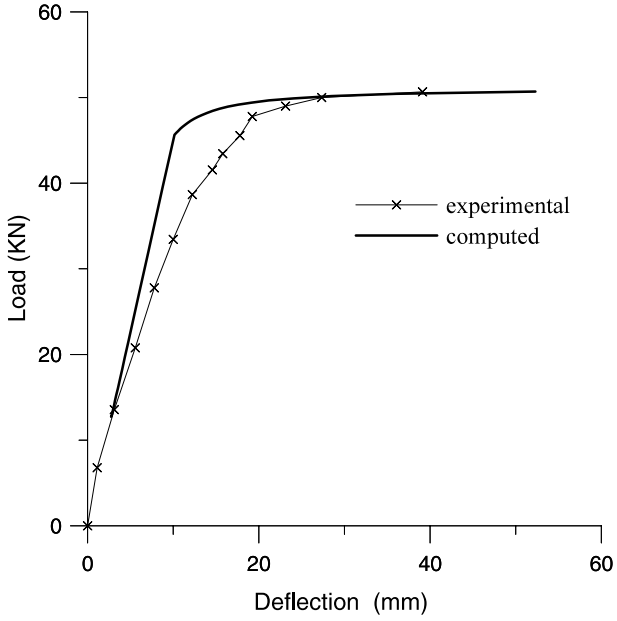

Fig. 6. Experimental and computed load vs. deflection diagrams for the beam DR30 [21].

on the observation that the fibers are fully effective if their direction is coaxial with the beam axis, and totally ineffective if they are directed along the other two orthogonal spatial directions. In addition, a further reduction must account for the fact that the fibers are not bisected by the crack, but intersected at a random point along their length [18]. For this reason the "effective density" of the fibers to be introduced in the model has been assumed equal to 0.2%, i.e. 1/5 of the real one.

These assumptions provide a brittleness number $N_P^{(2)}$

$$N_P^{(2)} = \frac{\gamma \sigma_u \sqrt{h}}{K_{IC}} = 0.84. \tag{37}$$

Finally, a rigid-perfectly plastic law is considered for the fibers. This assumption finds justification considering experimental results on similar steel fibers [19], see Fig. 7. As the experimental load vs. displacement diagrams have always positive slope with no slope discontinuities, the tension steel does not enter softening behavior and the fibers does not break along the crack depth, i.e. the crack opening is always less than the critical value w_c and the cohesive zone extends along the whole crack depth. In fact, when the critical opening w_c is achieved, the load vs. displacement diagram exhibits a softening branch, or at least a slope discontinuity. This is compatible with the fibers used in the experiment, as the crack opening at the maximum load is about 5 mm.

Consequently, the data used for running the numerical simulation of the beam DR32 are the two brittleness numbers (36) and (37), as the parameter $\widetilde{w}_c$ is not influent, being $\widetilde{w} < \widetilde{w}_c$. Fig. 8 reports the experimental load vs. displacement graphs compared to the computed ones, in both the cohesive or bridging option. The two curves are almost coincident, although in the two cases the nondimensional diagram bending moment vs. crack depth markedly differs, Fig. 9. As is expected for a given nondimensional moment, the crack depth is higher in the cohesive option. With reference to Fig. 9, once the value $\widetilde{M} = 1$ is

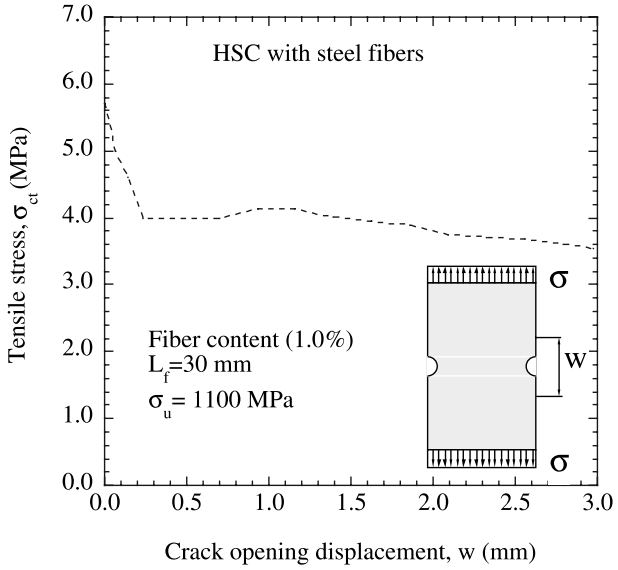

Fig. 7. Response of high-strength concrete with fibers, after Noghabai [19].

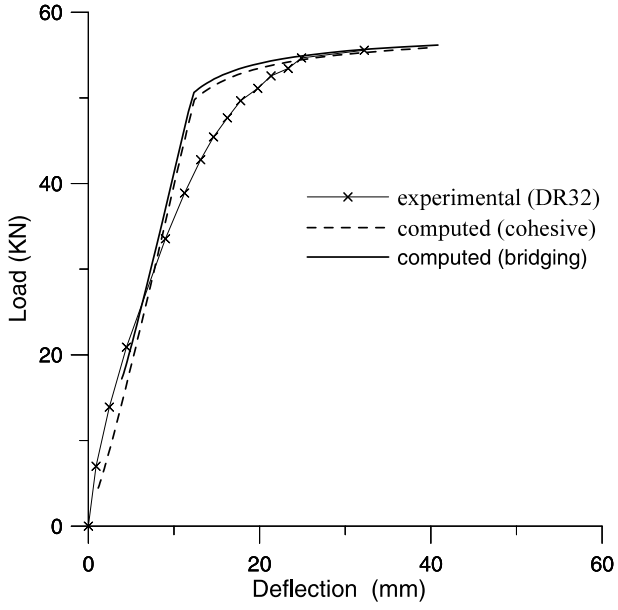

Fig. 8. Experimental and computed load vs. deflection diagrams for the beam DR32 [21].

fixed, a crack depth $\xi = 0.4376$ (bridging option) or $\xi = 0.5446$ (cohesive option) is found. The crack opening profiles are reported in Fig. 10.

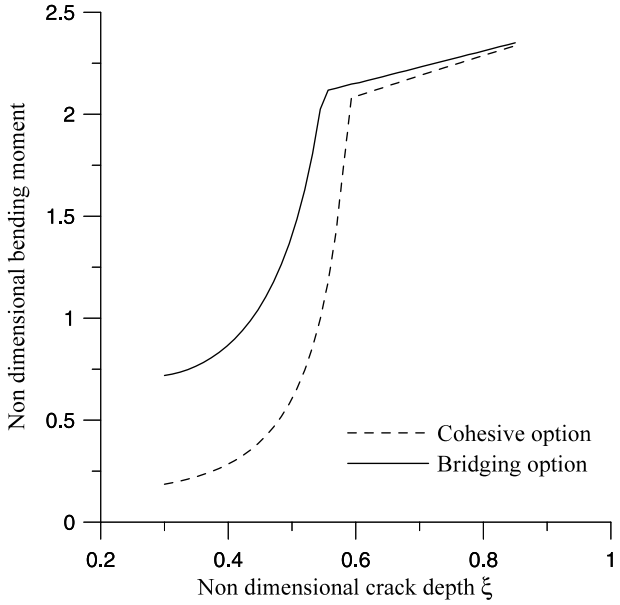

Fig. 9. Nondimensional bending moment vs. crack depth diagrams for the beam DR32.

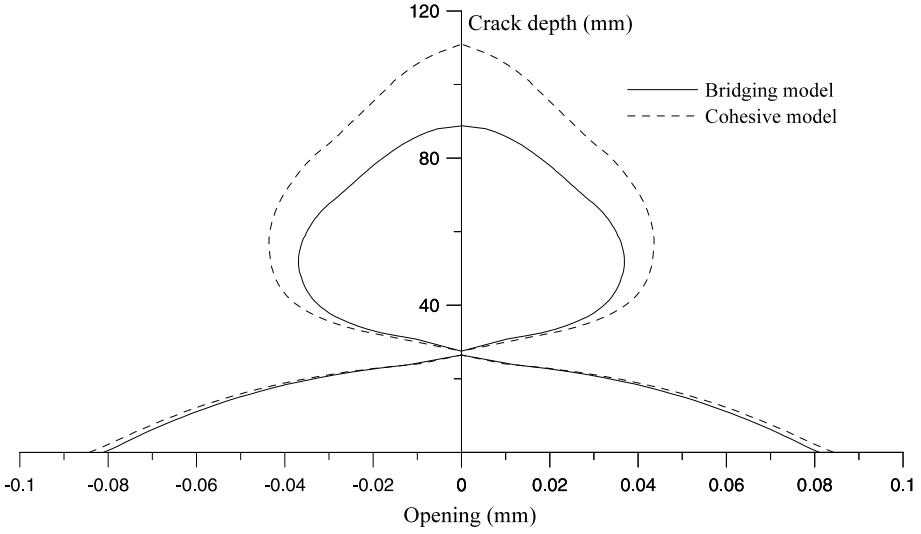

Fig. 10. Crack opening profile for the nondimensional bending moment $\tilde{M} = 1$.

7. Conclusions

The concurrent presence in a cementitious matrix of longitudinal bars and uniformly distributed fibers has been considered. Two different models have been proposed to simulate the flexural response of a concrete element: the *bridged crack model* and the *cohesive crack model*. In the bridged crack model the

composite material is theoretically simulated as a triphase material. Three distinct factors contribute to its global toughness: the cementitious matrix toughness K_{IC}, the fiber toughening mechanism, represented by the shielding effect $-K_{I\sigma}$ of the bridging tractions on the crack tip stress intensification and the reinforcement bars toughening mechanism represented by the factor $-K_{Ii}$.

In the cohesive crack model, on the other hand, the composite material is theoretically simulated as a twophase material. The global toughening mechanism of the matrix and the fibers is defined: the toughening mechanism peculiar of the matrix and explicitly represented in the bridged crack model by K_{IC} is merged with the toughening mechanisms developed in the process zone by the fibers.

In the bridged crack model the flexural behaviour is governed by three independent dimensionless parameters: $N_P^{(1)}$, $N_P^{(2)}$ and $\widetilde{w}_c$. In the cohesive crack model, on the other hand, the independent dimensionless parameters are only two, $N_P^{(1)}$, $N_P^{(2)}$, $\widetilde{w}_c$ being connected with $N_P^{(2)}$ through the Irwin's relationship.

Both the models reproduce satisfactorily the flexural behaviour of high-performance and/or fiber reinforced concrete members in bending. In particular, as the governing parameters are of easy physical meaning and of simple experimental evaluation, these models could represent a very useful tool for the study of mechanical properties (strength and ductility) and crack propagation regimes, based on concrete composition, typology and density of the fibers, distribution and characteristics of the longitudinal bars. The formulation justifies the dependence of the structural behaviour on the member size. Only when the brittleness numbers are the same, it is possible to obtain physically similar structural responses. When experimental results obtained on small specimens have to be extrapolated to full-scale structures, the reinforcement percentage, as well as the fiber volume ratio, should be scaled as $h^{0.5}$, the other mechanical parameters being fixed.

The numerical simulations of the experimental tests presented in this paper validate the model, which can be used to design the optimal mix of concrete, bars and fibers.

Acknowledgements

The present research was carried out with the financial support of the Ministry of University and Scientific Research (MURST), and of the EC-TMR contract no ERBFMRXCT 960062.

References

[1] Barenblatt GI. The mathematical theory of equilibrium cracks in brittle fracture. In: Dryden HL, von Karman T, editors. Advances in Applied Mechanics. New York: Academic Press; 1962. p. 55–129.
[2] Bosco C, Carpinteri A. Softening and snap-through behavior of reinforced elements. J Engng Mech (ASCE) 1992;118:1564–77.
[3] Bosco C, Carpinteri A. Discontinuous constitutive response of brittle matrix fibrous composites. J Mech Phys Solids 1995;43:261–74.
[4] Buckingham E. Model experiments and the form of empirical equations. Trans ASME 1915;37:263–96.
[5] Carpinteri A. Static and energetic fracture parameters for rocks and concrete. Mater Struct 1981;14:151–62.
[6] Carpinteri A. A fracture mechanics model for reinforced concrete collapse. Proceedings of the I.A.B.S.E. Colloquium on Advanced Mechanics of reinforced Concrete, Delft, 1981. p. 17–30.
[7] Carpinteri A. Stability of fracturing process in RC beams. J Struct Engng (ASCE) 1984;110:544–58.
[8] Carpinteri A, Ferro G, Ventura G. The bridged crack model for the analysis of fiber-reinforced composite materials. In: de Wilde WP, Blain WR, Brebbia CA, editors. Composite Materials and Structures. Southampton: WIT Press; 2000. p. 301–10.
[9] Carpinteri A, Ferro G, Bosco C, Elkathieb M. Scale effects and transitional phenomena of reinforced concrete beams. In: Carpinteri A, editor. Minimum Reinforcement in Concrete Members. Oxford: Elsevier Science; 1999. p. 1–30.
[10] Carpinteri A, Massabó R. Bridged versus cohesive crack in the flexural behavior of brittle–matrix composites. Int J Fract 1996;81:125–45.
[11] Carpinteri A, Massabó R. Continuous vs. discontinuous bridged-crack model for fiber-reinforced materials in flexure. Int J Solids Struct 1997;34:2321–38.

[12] Carpinteri A, Massabó R. Reversal in failure scaling transition of fibrous components. J Engng Mech (ASCE) 1997;123:107–14.
[13] Cox BN, Mashall DB. Concepts for bridged cracks in fracture and fatigue. Acta Metallurgica et Materialia 1994;42:341–63.
[14] Ferro G. Multilevel bridged crack model for high-performance concretes. Theor Appl Fract Mech 2002;38:177–90.
[15] Karihaloo BL, Wang J, Grzybowski M. Doubly periodic arrays of bridged cracks and short fibre reinforced cementitious composites. J Mech Phys Solids 1996;44:1565–86.
[16] Jenq YS, Shah SP. Crack propagation in fiber-reinforced concrete. J Engng Mech (ASCE) 1986;112:19–34.
[17] Lange-Kornbak D, Karihaloo BL. Design of plain concrete moxes for minimum brittleness. Adv Cem Based Mater 1998;3:124–32.
[18] Li VC, Wang Y, Backer S. A micromechanical model of tension-softening and bridging toughening of short random fiber reinforced brittle matrix composites. J Mech Phys Solids 1991;39:607–25.
[19] Noghabai K. Beams of fibrous concrete in shear and bending: experiment and model. J Struct Engng (ASCE) 2000;126:243–51.
[20] Okamura H, Watanabe K, Takano T. Deformation and strength of cracked member under bending moment and axial force. Engng Fract Mech 1975;7:531–9.
[21] Swamy RN, Al-Ta'an SA. Deformation and ultimate strength in flexure of reinforced beams made with steel fiber concrete. ACI J 1981;5:395–405.
[22] Tada H, Paris PC, Irwin G. The Stress Analysis of Cracks Handbook. Paris Productions Incorporated (and Del Research Corporation), St. Louis, Missouri, 1963.